Prediction of Radiative Heat Transfer in Industrial Equipment Using the Radiation Element Method

Zhixiong Guo
Assistant Professor,
Mechanical and Aerospace Engineering,
Rutgers, The State University of New Jersey,
New Brunswick, NJ 08854
e-mail: guo@thebrain.rutgers.edu

Shigenao Maruyama
Institute of Fluid Science,
Tohoku University,
Sendai 980, Japan
e-mail: maruyama@ifs.tohoku.ac.jp

The radiation element method by ray emission method, REM^2, has been formulated to predict radiative heat transfer in three-dimensional arbitrary participating media with nongray and anisotropically scattering properties surrounded by opaque surfaces. To validate the method, benchmark comparisons were conducted against the existing several radiation methods in a rectangular three-dimensional media composed of a gas mixture of carbon dioxide and nitrogen and suspended carbon particles. Good agreements between the present method and the Monte Carlo method were found with several particle density variations, in which participating media of optical thin, medium, and thick were included. As a numerical example, the present method is applied to predict radiative heat transfer in a boiler model with nonisothermal combustion gas and carbon particles and diffuse surface wall. Elsasser narrow-band model as well as exponential wide-band model is adopted to consider the spectral character of CO_2 and H_2O gases. The distributions of heat flux and heat flux divergence in the boiler furnace are obtained. The difference of results between narrow-band and wide-band models is discussed. The effects of gas model, particle density, and anisotropic scattering are scrutinized.
[DOI: 10.1115/1.1388235]

Introduction

In recent decade, significant progress has been made in development of solution methods for multi-dimensional radiative heat transfer in absorbing, emitting, and scattering participating media [1]. However, it is usually a formidable task if the nongray and anisotropic scattering characters of the medium are accounted for, as pointed out by Farmer and Howell [2]. Furthermore, it is frequently difficult to apply these methods to complex three-dimensional configurations such as that used in finite element analysis, except the Monte Carlo method which may be extremely time-consuming, and the results are subject to statistical error. The radiation element method by ray emission model proposed by Maruyama [3] and Maruyama and Aihara [4] is an extension of zone method and is a generalized numerical method for analyzing radiation transfer in participating media and specular and/or diffuse surfaces with arbitrary configurations and thermal conditions. This method was applied to very complicated configurations, e.g., the applications to a large device for nuclear fusion reactor [5] and a Czochralski crystal growth furnace [6].

Accurate prediction of thermal radiation in combustion chamber is of practical importance. However, many investigators in the combustion field did not take nongray and anisotropic scattering characteristics into account. The assumption of isotropic scattering used by Fiveland and Latham [7] is somewhat questionable as pointed out by Fiveland and Wessel [8]. It is also well known that the use of gray assumption is not appropriate for gas radiation [9]. The wide-band model is widely employed in radiation transfer in combustion [7]. However, the wide-band model has not been compared with the narrow-band model in realistic problems.

An instinctive weakness in REM^2 method is the requirement of isotropic scattering phase function [4]. However, this problem can be solved with ease by an appropriate scaling technique. There are numerous ways to scale a complex anisotropic scattering, such as δ-M method [10]. The validity of the scaling approximation and its high accuracy have been verified by many researchers [11,12]. Maruyama has applied the zeroth-order delta function approximation to REM^2 for the case of plane parallel system with very good accordance with exact solution, even for strong forward scattering particles [13,14].

In this paper, the REM^2 is developed to incorporate the radiation properties of spectral dependence with narrow-band model and anisotropic scattering of particles. The temperature and radiative properties should be uniform in each radiation element, but can be inhomogeneous among radiation elements. The view factors are attained by ray tracing method in which path lengths in each radiation element can be specified; thus, all gas models are feasible in the present method to account for the nongray characteristics of participating gas. For the sake of benchmark comparison, the Elsasser narrow-band model is employed in conjunction with the exponential wide-band model [15]. The present REM^2 approach was firstly applied to radiation transfer in three-dimensional rectangular media involving CO_2 and nitrogen gas mixture and anisotropic scattering carbon particles. The validity and sensitivities of the present method were verified by the existing Monte Carlo calculation of Farmer and Howell [2] and several other methods [1,16,17]. Its calculation efficiency was compared with the YIX method [16].

As a numerical example of application in complicated system of arbitrary shape, the radiative heat transfer is demonstrated in a three-dimensional boiler furnace. The Elsasser narrow-band model (NBM) as well as the exponential wide-band model (WBM) is adopted to consider the spectral character of CO_2 and H_2O gases. The results of heat flux on the walls and heat flux divergence in the boiler are compared between the narrow-band model and the wide-band model. The effect of the anisotropic scattering is also discussed.

Contributed by the Pressure Vessels and Piping Division for publication in the JOURNAL OF PRESSURE VESSEL TECHNOLOGY. Manuscript received by the PVP Division, November 6, 2000; revised manuscript received May 23, 2001. Associate Editor: Y. W. Kwon.

Mathematical Formulation

To consider a radiation element of participating medium, as shown in Fig. 1, the spectral radiation intensity I_λ at $\mathbf{r}$ in the direction $\hat{s}$ can be formulated as

$$\frac{dI_\lambda(\mathbf{r},\hat{s})}{dS} = -(\kappa_\lambda+\sigma_{s,\lambda})I_\lambda(\mathbf{r},\hat{s}) + \kappa_\lambda I_{b,\lambda}(T) + \frac{\sigma_{s,\lambda}}{4\pi}\int_{4\pi} I_\lambda(\mathbf{r},\hat{s}')\Phi_\lambda(\hat{s}'\to\hat{s})\mathrm{d}\omega \quad (1)$$

where κ_λ and $\sigma_{s,\lambda}$ are spectral absorption and scattering coefficients, respectively, and $\Phi_\lambda(\hat{s}'\to\hat{s})$ is the phase function.

The following assumptions are introduced to simplify the problem: 1) Each element is at a constant uniform temperature. The refractive index and heat generation rate per unit volume are also constant and uniform over the polyhedral radiation element. 2) Scattering in the participating medium is isotropic, while scaling technique is employed for anisotropic scattering. 3) The scattering radiation distributes uniformly over the element. The third term of the right-hand side of Eq. (1) is approximated as

$$\frac{\sigma_{s,\lambda}}{4\pi}\int_{4\pi} I_\lambda(\mathbf{r},\hat{s}')\Phi_\lambda(\hat{s}'\to\hat{s})\mathrm{d}\omega = \frac{\sigma_{s,\lambda}}{4\pi}\int_{4\pi} I_\lambda(\mathbf{r},\hat{s}')\mathrm{d}\omega = \sigma_{s,\lambda}I_\lambda^D \quad (2)$$

where I_λ^D is the averaged diffuse radiant intensity. It should be noted that I_λ^D is similar to diffuse radiosity that was used for radiation transfer of arbitrary diffuse and specular surfaces [3]. Bringing the extinction coefficient β_λ and albedo Ω forward, Eq. (1) is rewritten as

$$\frac{\mathrm{d}I_\lambda(\mathbf{r},\hat{s})}{\mathrm{d}S} = \beta_\lambda[-I_\lambda(\mathbf{r},\hat{s}) + (1-\Omega)I_{b,\lambda}(T) + \Omega I_\lambda^D] \quad (3)$$

If the albedo Ω is redefined as Ω^D and the specular reflectivity of surface element Ω^S is defined, a generalized form of the spectral radiant energy of element i, which may be either a volume or a surface element, can be expressed as follows:

$$Q_{J,i,\lambda}(\hat{s}) = [(1-\Omega_i^D-\Omega_i^S)I_{b,i,\lambda}(T_i) + \Omega I_{i,\lambda}^D] \times \int_{4\pi} A_i(\hat{s})\left[1-\exp\left(-\int_0^S \beta_{i,\lambda}dS'\right)\right]\mathrm{d}\omega \quad (4)$$

Surface element and volume element are distinguished by the conditions $\int_0^S \beta_{i\lambda}dS' \gg 1$ and $\Omega_i^S = 0$, respectively.

To simplify the integration in Eq. (4), we introduce an effective radiation area A_i^R as

$$A_i^R = \frac{1}{\pi}\int_{4\pi} A_i(\hat{s})\left[1-\exp\left(-\int_0^{\bar{S}}\beta_{i,\lambda}\mathrm{d}S'\right)\right]\mathrm{d}\omega \quad (5)$$

where an averaged thickness of the radiation element in the direction $\hat{s}$ was introduced as

$$\bar{S} = V/A(\hat{s}) \quad (6)$$

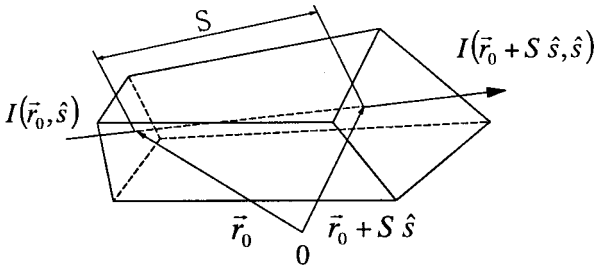

Fig. 1 Attenuation of radiation passing through an element

in which, V and $A(\hat{s})$ are the volume and area projected onto the surface normal to $\hat{s}$, respectively. The rate of spectral radiation energy emitted and isotropically scattered by the radiation element can be expressed in a generalized form as

$$Q_{J,i,\lambda} \equiv A_i^R(\varepsilon_i E_{b,i,\lambda} + \Omega_{i,\lambda}^D G_{i,\lambda}) \quad (7)$$

where $\varepsilon_i = 1-\Omega_i^D-\Omega_i^S$, $E_{b,i,\lambda} = \pi I_{b,i,\lambda}$, $G_{i,\lambda} = \pi I_{i,\lambda}^D$, and $Q_{J,i,\lambda}$ is the diffuse radiation transfer rate. It should be noted that the value A_i^R is a function of wavelength for a nongray participating medium. The net rate of heat generation can be derived from the heat balance on the radiation element as

$$Q_{X,i,\lambda} = A_i^R\varepsilon_i(E_{b,i,\lambda} - G_{i,\lambda}) \quad (8)$$

The expressions of heat transfer rates of irradiation energy $Q_{G,i,\lambda}$ and emissive power $Q_{T,i,\lambda}$ of the radiation element are

$$Q_{G,i,\lambda} \equiv A_i^R G_{i,\lambda}, \quad Q_{T,i,\lambda} = A_i^R\varepsilon_i E_{b,i,\lambda} \quad (9)$$

If the system is consisted of N volume and surface elements, then Eqs. (7) and (8) can be rewritten as

$$\left.\begin{aligned} Q_{J,i,\lambda} &= Q_{T,i,\lambda} + \sum_{j=1}^N F_{j,i}^D Q_{J,j,\lambda} \\ Q_{X,i,\lambda} &= Q_{T,i,\lambda} - \sum_{j=1}^N F_{j,i}^A Q_{J,j,\lambda} \end{aligned}\right\} \quad (10)$$

in which, the absorption view factor $F_{i,j}^A$ and diffuse scattering view factor $F_{i,j}^D$ are introduced as defined by Maruyama and Aihara [4]. The heat transfer rate of spectral emissive power $Q_{T,i,\lambda}$ for each radiation element is given as a boundary condition. The unknown $Q_{X,i,\lambda}$ can be obtained by solving Eq. (10). The total net rate of heat generation is obtained as

$$Q_{X,i} = \int_0^\infty Q_{X,i,\lambda}\mathrm{d}\lambda \quad (11)$$

The heat flux of a surface element or the heat flux divergence of a volume element is calculated by

$$q_{X,i} = Q_{X,i}/A_i \quad \text{or} \quad q_{X,i} = Q_{X,i}/V_i \quad (12)$$

The radiation elements consisted of numerous polygons and polyhedrons can be produced by applying general-purpose pre and post-processor packages for the finite element method, e.g., PATRAN. The view factors are calculated by ray tracing method [18]. The ray emission model is the same as used by Maruyama and Aihara [4]. The discrete directions were distributed uniformly over the entire solid sphere. If the total number of emitted rays is Nr, the discrete solid angle is $\Delta\omega = 4\pi/Nr$.

Spectral Optical Properties

The Elsasser narrow-band model is used in conjunction with the correlation parameters in Edwards wide-band model [15] to determined the spectral absorption coefficients of CO_2 and H_2O, which is given as follows:

$$a_\eta = \rho\frac{S_c}{\delta}\frac{\sinh(\pi\beta/2)}{\cosh(\pi\beta/2)-\cos[2\pi(\eta-\eta_c)/\delta]} \quad (13)$$

where

$$\frac{S_c}{\delta} = \frac{\alpha}{\omega}\exp[-(a/\omega)|\eta-\eta_c|] \quad (14)$$

$$\beta = \frac{C_2^2 P_e}{4C_1C_3} \quad (15)$$

$$\alpha = C_1 \quad (16)$$

$$\omega = C_3 \quad (17)$$

$$\delta = 30C_3 \quad (T = 100\,[\mathrm{K}]) \tag{18}$$

where C_1, C_2, and C_3 are the correlation parameters and given by Siegel and Howell [19]. Then, the apparent extinction coefficient of element in the direction $\hat{S}$ is obtained as a function of the averaged path length as follows:

$$\beta_g = \ln\left[\int_{-\delta/2}^{\delta/2} \exp(-a_\eta \bar{S})\,\mathrm{d}\eta\right] \tag{19}$$

The particles are assumed to be carbon spheres with a diameter of 30 μm. Mie theory and the optical constants for carbon specimen no. 2 in Foster and Howarth [20] were used to compute scattering and extinction efficiencies. The values are listed in Table 1 of Tong and Skocypec [1]. The scattering phase function is approximated by a delta-Eddington function as [21]

$$P(\Psi) = 2f\delta(1-\cos\theta) + (1-f)(1+3g\cos\theta) \tag{20}$$

where $f = 0.111$ and $g = 0.215$.

As mentioned in the introduction, however, Eq. (2) requires the assumption of isotropic scattering. The phase function Eq. (20) was scaled to zeroth-order delta function approximation as discussed in Maruyama [13,14]. The scaled extinction coefficient β_P^* and albedo Ω^D are

$$\beta_P^* = \beta_P(1-a_1\Omega/3), \quad \Omega^D = \frac{\Omega(1-a_1/3)}{1-a_1\Omega/3} \tag{21}$$

where a_1 is a coefficient of the first term in Legendre polynomials. The final extinction coefficient of the mixture of particles and gases is expressed as

$$\beta = \sum_{k=1}^{N_g} \beta_{gk} + \beta_P^* \tag{22}$$

where β_{gk} is the apparent extinction coefficient of the kth gas, and N_g is the total number of gas components.

Results and Discussion

Three-Dimensional Enclosure. The present method is firstly applied to solve radiation heat transfer in a three-dimensional rectangular medium as shown in Fig. 2. The participating medium is a mixture of CO_2 and N_2 gases and carbon particles. The total mixture pressure is specified to be 1 atm, with a volume fraction of CO_2 of 0.21. The temperature of the medium is constant and uniform at 1000 K. The enclosure is covered with black and cold surface. Since this is a symmetric problem, a one-eighth symmetric analysis model is considered in calculation, in which three symmetric surfaces are specified as totally specular reflection of $\Omega^s = 1$. The analysis model includes 216 volume elements, 108 black surface elements, and 108 perfect mirror elements.

The present calculations are compared with the results of several other solution methods for several carbon particle densities of $Nc = 2.0\times10^7$, 2.0×10^8, and 2.0×10^9 particles per cubic meter, which represent participating media of optical thin, medium, and thick, respectively. The benchmark comparison of radiative heat flux is shown in Fig. 3. The results of the Monte Carlo method, the YIX method, and the GZX Method are from Farmer and Howell [2], Hsu et al. [16], and Yuen et al. [17], respectively. Good agreements are found among the simulations of the Monte Carlo, the YIX, and the present methods. In particular, the present calculation is the closest to the results of the Monte Carlo of Farmer and Howell [2] in the cases of optical thin ($Nc = 2.0\times10^7$) and optical thick ($Nc = 2.0\times10^9$). Comparing these two methods, the general error is 5 percent. For $Nc = 2.0\times10^8$, the difference increases to 10 percent in the boundary area. The present predictions are generally lower than those of Farmer and Howell [2] and Hsu et al. [16], but are higher than the predictions of Yuen et al. [17].

The divergence of radiative heat flux is displayed in Fig. 4, in which comparisons are performed between the present method and the Monte Carlo method [2] in the same conditions of Fig. 3. In all the cases of three particle densities, the present results agree

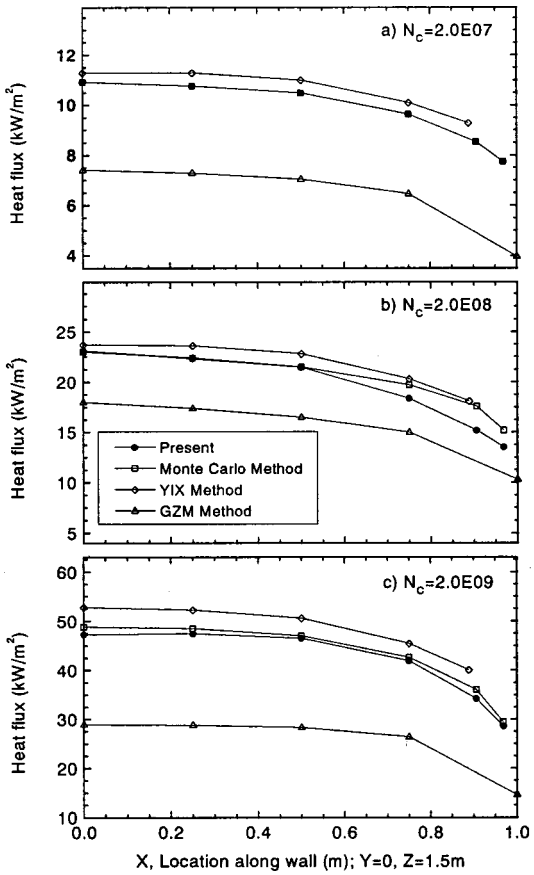

Fig. 3 Comparison of heat flux at $Y=0$ and $Z=1.5$ m

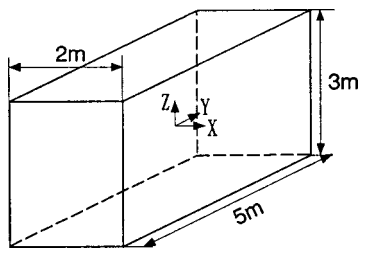

Fig. 2 Geometry of a rectangular medium

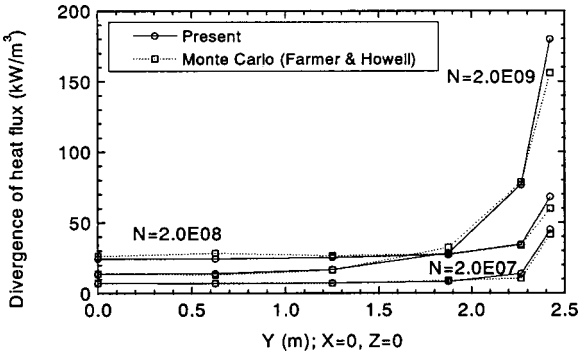

Fig. 4 Comparison of divergence of heat flux

Table 1 Comparison of CPU time

CPU time [sec]	$Nc = 2.0\times10^7$	$Nc = 2.0\times10^8$	$Nc = 2.0\times10^9$
YIX*	1317	2284	5267
Present**	789	786	773

* Cray Y-MP/864; ** Cray C-916.

well with those of Monte Carlo. The difference between the two solutions is basically within 10 percent. However, an error of 20 percent exists in the boundary area.

The computation efficiency is a major concern in three-dimensional radiation solutions. The calculation CPU time is available for the YIX method [16], in which the computation was performed on a Cray Y-MP/864 supercomputer.

In the present computation, a Cray C-916 supercomputer was employed. The most time-consuming part of the calculation was the ray tracing process. This portion in the program was not vectorized. Neither parallel technique was used. The CPU time (1 CPU) for the two solutions is listed in Table 1. No direct comparison is available due to different computers used in the two methods. However, it should be noted that the trends of CPU time in accordance with the particle density are different between the two approaches. When the particle density increases, i.e., the participating media changes from optical thin to optical thick, the CPU time increases enormously in the YIX method, while a slight decrease of CPU time is found in the present method. This is due to the ray tracing time decreases as the medium optical length increases.

In the foregoing calculation cases, the number of ray emission bundles was set to be $Nr=155$. The influence of ray emission number is demonstrated in Fig. 5, in which the radiative heat flux and divergence of heat flux are illustrated in the case of $Nc=2.0\times10^9$ for $Nr=45$, 155, and 561, respectively. It is seen that the ray effect [22], which causes errors in analysis of a complicated geometry by the discrete ordinate method, is minimized in the present method. This is because the calculation of view factors is corrected using a method similar to that of Omori et al. [23] and the number of ray emission in the present solution is usually much larger than that used in the discrete ordinate method.

Radiation Transfer in a Boiler Model. The present method has advantages over other solutions except the Monte Carlo method in dealing with radiation transfer in arbitrary geometry. As a numerical example of complicated configuration, radiative heat transfer in a boiler furnace was investigated. A practical boiler configuration of 125 MW(e) is presented in Fig. 6 [9] with ASTM No. 6 heavy oil fed from two opposite side walls. The boiler is operated in atmospheric pressure. The temperature of the boiler wall is 623 K. In the gas exit region, the wall temperature is high since a reheater is usually located. It is given to be 813 K. The wall surfaces are diffuse with diffuse reflectivity of 0.8. A temperature profile inside the boiler was modeled according to the result of Aoki et al.[9] as expressed by the following equations: When $Z\geqslant H_1$

$$T=T_0\left[a_1\left(1-\frac{|2X-W_1|}{2W-W_1}\right)\left(1-\frac{|2Y-L|}{2L}\right)\left(1-\frac{|Z-H_1|}{H-H_1}\right)+b_1\right] \tag{23}$$

When $Z<H_1$

$$T=T_0\left[a_2\left(1-\frac{|2X-W|^3}{W^3}\right)\left(1-\frac{|2Y-L|}{10L}\right)\left(1-\frac{|2Z-H_1|}{10H_1}\right)+b_2\right] \tag{24}$$

in which, $a_1=1$, $b_1=2.5$, $a_2=2.8$, $b_2=1$, and the input fuel temperature $T_0=563$ K.

The combustion gas is composed of CO_2, H_2O, and N_2 with the mole fractions of CO_2 and H_2O being 0.119 and 0.085, respectively. The profile of the combustion gas is assumed to be uniform all over the boiler. According to the measurement of Smyth et al. [24], the soot inception region in flame is found to occur at the high-temperature edge with maximum intensity in a region at 1300~1650 K. Carbon particles in the present model are assumed to produce in a region which satisfies the expression of

$$\begin{cases} 1000\ \text{K}\leqslant T\leqslant 2000\ \text{K} \\ H_1/9\leqslant Z\leqslant 6H_1/9 \end{cases} \tag{25}$$

The particle fraction is assumed to be uniform in the particle region. Three cases of particle concentration of $Nc=2.0\times10^7$, 2.0×10^8, and 2.0×10^9 particles per cubic meter are considered.

The division grid of radiation element of boiler is also shown in Fig. 6. The total element number in the boiler is 2142, which includes 1360 volume elements and 782 surface elements located on the furnace wall. In actual calculation, a half-symmetrical analysis model is adopted since the boiler is symmetric along the center plane of $Y=L/2$. The number of ray emissions for a radiation element is set to be $Nr=155$. All calculations were performed in SX-4/128H4 supercomputer.

At first, the effect of anisotropic scattering of particles is investigated. The heat flux distributions on the wall and the divergence of heat flux at the center plane of the boiler are illustrated in Figs. 7(*a*) and (*b*), respectively, for anisotropic scattering (left) and isotropic scattering (right) in the case of particle concentration of $Nc=2.0\times10^9$. The heat flux and the divergence of heat flux in Figs. 7–9 are normalized by $-\sigma T_N^4$ and $\sigma T_N^4/W$, respectively, with $T_N=2000$ [K]. The negative value of heat flux represents that the heat is from participating medium transfer into wall surface. In the present radiative heat transfer, the divergence of heat

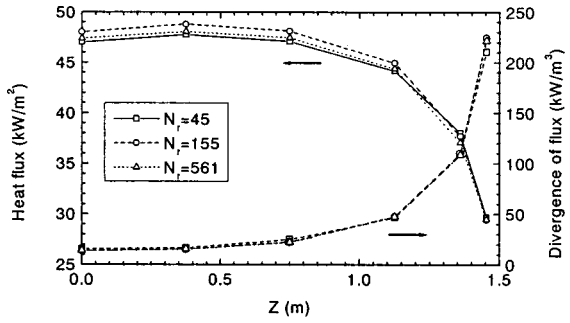

Fig. 5 Effect of ray emission number

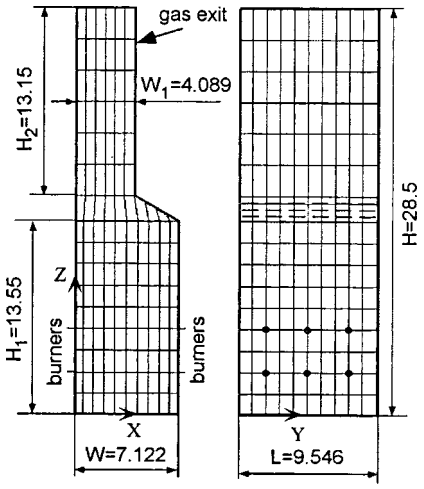

Fig. 6 Geometry and grid arrangement of a boiler model

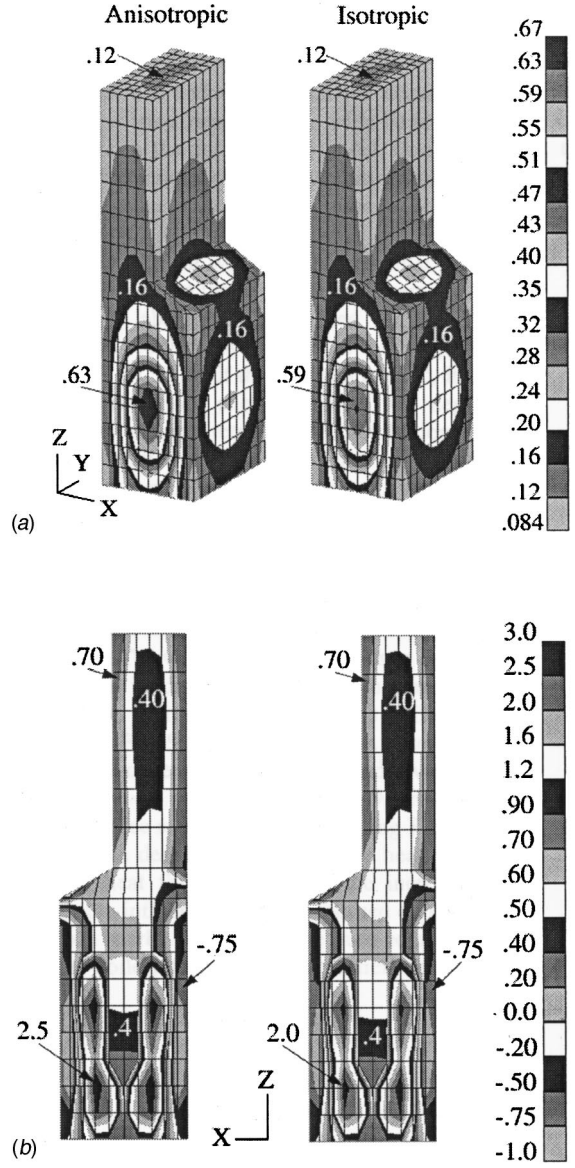

Fig. 7 Comparison between anisotropic scattering and isotropic scattering with $N_c = 2.0 \times 10^9$—(*a*) distribution of normalized heat flux, (*b*) normalized heat flux divergence at $Y = L/2$

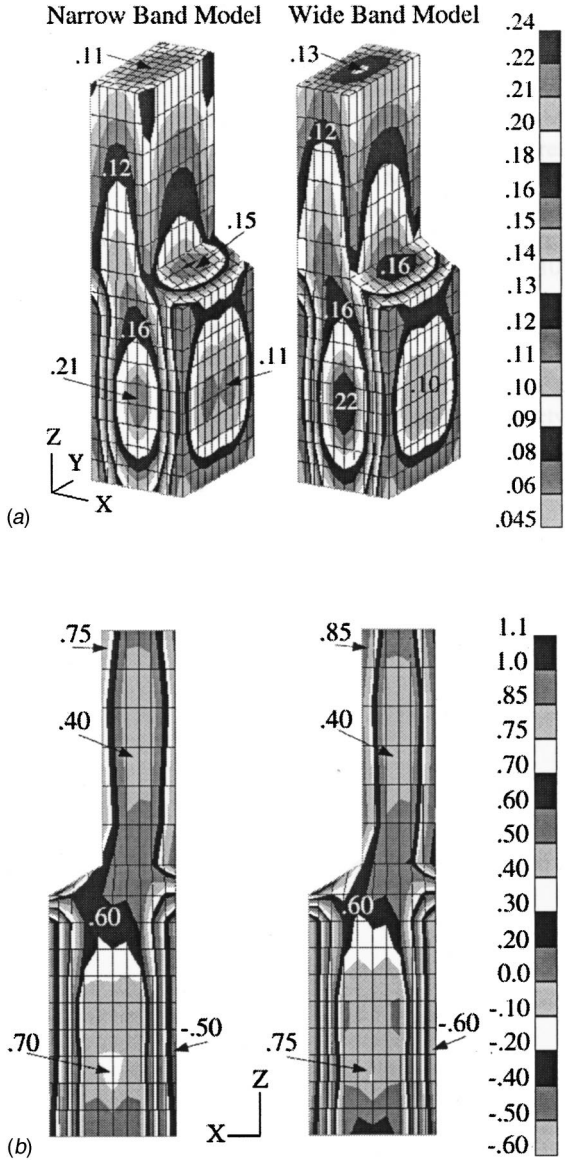

Fig. 8 Comparison between narrow-band model (NBM) and wide-band model (WBM) with $N_c = 2.0 \times 10^7$—(*a*) distribution of normalized heat flux, (*b*) normalized heat flux divergence at $Y = L/2$

flux is the same as heat production per unit volume. As for the divergence of heat flux, a negative value means absorbing heat, while a positive value stands for heat generation. It is seen that larger heat flux is distributed in the wall surfaces near the fire region, while the heat flux on the surfaces in pure combustion gas and gas exit regions is very low. This reveals that the radiation from high-temperature particles is much stronger than that from high-temperature combustion gas, especially for the case of larger number density of the particles. Comparing the results between anisotropic and isotropic scatterings in the particle region in Figs. 7(*a*) and (*b*), it was found that the heat flux as well as the divergence of heat flux increased when the anisotropic property was accounted for. The difference of the results between the anisotropic and isotropic scatterings is generally 15 percent. There are some points where the difference is about 30 percent. In the present model, no particles exist in the central part of the fire according to the assumption of soot production, Eq. (25). As in the practical case, fire is turbulent flame and soot is produced in the whole region of fire. In such a case, the prediction difference between anisotropic and isotropic scattering would increase.

The comparison of numerical results of heat flux and heat flux divergence between gas models of narrow band and wide band is demonstrated in Fig. 8 in the case of $Nc = 2.0 \times 10^7$ with anisotropic scattering. The foregoing Elsasser narrow-band model is used in conjunction with the correlation parameters in a wide-band model. The Edwards exponential wide-band model [15] is used as a wide-band model. The absorption coefficient calculated by these gas models were compared with LBL solution by Maruyama et al. [25]. It was shown that the solution of the narrow-band model agrees with that of LBL and was more accurate than that of the wide-band model. It is seen that the gas model has active effect on the accuracy of numerical prediction. The predicted results by the wide-band model are generally larger than those by the narrow-band model. Comparing two different models, the differences of heat flux are about 10 percent, while the differences of divergence of heat flux increase to 20 percent, with 40 percent detected in some positions.

In both Figs. 7(*b*) and 8(*b*), it was seen that negative values of divergence of heat flux appeared in the region near burners and air

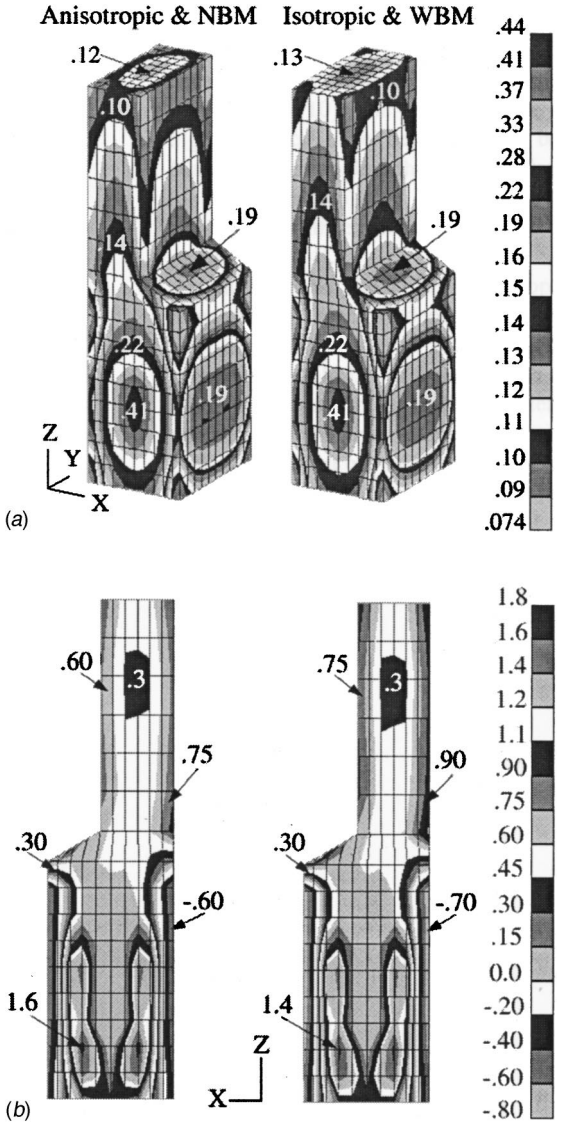

Fig. 9 Comparison between solutions of anisotropic and NBM and of isotropic and WBM with $N_c = 2.0\times10^8$—(*a*) distribution of normalized heat flux, (*b*) normalized heat flux divergence at $Y = L/2$

ports. This radiation energy absorption is caused by the low-temperature combustion gas cooled by the input of very low-temperature fuel and air (563 K). Thus, if the fuel is premixed, it can be heated by absorbing radiation energy. Since we neglect convection heat transfer and assume temperature distribution, the calculated value of heat generation rate or divergence of radiative heat flux may not describe the realistic value; however, this heat absorption region will appear in a real boiler.

Finally, the comparison is extended to solutions with anisotropic scattering and the narrow-band model and with isotropic scattering and the wide-band model. Figure 9 portrays the comparisons of heat flux on the wall and heat flux divergence in the center plane for particle density $Nc = 2.0\times10^8$. The wide-band model tends to increase the prediction of heat flux and its divergence; on the other hand, the effect of isotropic scattering is reversed. Hence, the differences between the two solutions in Fig. 9 are not so large as observed in Figs. 7 and 8. In general, 10 percent difference of heat flux and divergence of heat flux is found. However, in the case of Fig. 9, maximum difference of heat flux divergence reaches 30 percent. Comparing Figs. 7–9, the influence of particle density is revealed. The heat flux as well as the divergence of heat flux increases as the increase of particle density. However, the influence is mainly focused on the fire region and the wall surface nearby the fire. In the pure combustion gas region in the top of the boiler, the influence of particle density is very weak.

Conclusions

To predict radiative heat transfer in three-dimensional arbitrary participating media with nongray and anisotropically scattering properties, the radiation element method by ray emission method, REM^2, has been used. As benchmark comparisons, radiative heat transfer of rectangular media was predicted by the present method. Good agreements between the present method and the Monte Carlo method were found in the cases of participating media of optical thin, medium, and thick. But the calculation CPU time by the present method is shorter by several factors than that by the Monte Carlo method. Furthermore, the calculation of a participating medium of optical thick does not require longer CPU time than that of optical thin medium compared with the YIX method.

As a numerical example of arbitrary shape and engineering application, radiative heat transfer in a boiler model with non-isothermal nongray combustion gas and anisotropic scattering carbon particles has been investigated. Emphasis was placed on the discussion of the influences of gas models and scattering characteristics. The use of wide-band model increases the heat flux and divergence of heat flux by a range of 10 to 40 percent compared with the results by employing the narrow-band model, while the assumption of isotropic scattering decreases the prediction by 10 to 30 percent of the anisotropic scattering. As the increase of the particle density, the radiative heat flux and the divergence of heat flux increase.

Acknowledgments

The authors would like to express their gratitude to Professor John R. Howell of the University of Texas at Austin and Dr. Takeru Fukuchi of Kure Research Lab. in Babcoch-Hitachi for their useful information. The first author is grateful for the discussion on boiler model with Dr. Hideyuki Aoki and Mr. Juongming Ruan of Tohoku University.

Nomenclature

A = area
A^R = effective radiation area, Eq. (5)
a = band symmetry factor, Eq. (13)
E_b = blackbody emissive power
f = coefficient of scattering phase function, Eq. (20)
$F^A_{i,j}$ = absorption view factor from element i to j
$F^D_{i,j}$ = diffuse scattering view factor
H = height [m]
I = radiation intensity
I^D_λ = diffuse radiant intensity
L = length [m]
N = no. of element
Nc = density of carbon particles
Nr = no. of ray emission bundles
P_e = gas band correlation parameter
Q_G = heat transfer rate of irradiation, Eq. (9)
Q_T = heat transfer rate of emissive power, Eq. (9)
Q_J = heat transfer rate of diffuse radiosity, Eq. (4)
Q_X = net heat transfer rate of heat generation, Eq. (8)
q_X = heat flux for surface element or divergence of heat flux for volume element, Eq. (12)
$\mathbf{r}$ = position vector
S = path length through element
$\underline{S}$ = averaged thickness of element in direction $\hat{S}$

$\mathbf{s}$ = unit direction vector
S_c = mean line intensity, Eq. (14)
T = temperature
V_i = volume of element i
W = width [m]
X,Y,Z = coordinates
α = band intensity, Eq. (16)
β = extinction coefficient; pressure broadening parameter
δ = Dirac-delta function; absorption line spacing
ε = emissivity, $\equiv 1-\Omega^D-\Omega^S$
κ = absorption coefficient
λ = wavelength
Φ = scattering phase function
η = wave no.
θ = scattering angle
Ω^D = albedo of volume element or diffuse reflectivity of surface element, respectively
Ω^S = specular reflectivity
ω = solid angle; bandwidth parameter
σ = Stefan-Boltzmann constant
σ_S = scattering coefficient

Subscripts

b = blackbody
g = gas
i = element i
j = element j
P = particle
λ = spectral value

References

[1] Tong, T. W., and Skocypec, R. D., 1992, ''Summary on Comparison of Radiative Heat Transfer Solutions for a Specified Problem,'' *Developments in Radiative Heat Transfer*, ASME HTD-Vol. 203, pp. 253–258.

[2] Farmer, J. T., and Howell, J. R., 1994, ''Monte Carlo Prediction of Radiative Heat Transfer in Inhomogeneous, Anisotropic, Nongray Media,'' J. Thermophys. Heat Transfer, **8**, pp. 133–139.

[3] Maruyama, S., 1993, ''Radiation Heat Transfer Between Arbitrary Three-Dimensional Bodies with Specular and Diffuse Surfaces,'' Numer. Heat Transfer, Part A, **24**, pp. 181–196.

[4] Maruyama, S., and Aihara, T., 1997, ''Radiation Heat Transfer Between Arbitrary Three-Dimensional Absorbing, Emitting and Scattering Media and Specular and Diffuse Surfaces,'' ASME J. Heat Transfer, **119**, pp. 129–136.

[5] Maruyama, S., and Higano, M., 1997, ''Radiative Heat Transfer of Torus Plasma in Large Helical Device by Generalized Numerical Method REM^2,'' Energy Convers. Manage., **38**, pp. 1187–1195.

[6] Guo, Z., Maruyama, S., and Tsukada, T., 1997, ''Radiative Heat Transfer in Curved Specular Surface in Czochralski Crystal Growth Furnace,'' Numer. Heat Transfer, Part A, **32**, pp. 595–611.

[7] Fiveland, W. A., and Latham, C. E., 1993, ''Use of Numerical Modeling in the Design of a Low-NO_x Burner for Utility Boilers,'' Combust. Sci. Technol., **93**, pp. 53–72.

[8] Fiveland, W. A., and Wessel, R. A., 1988, ''Numerical Model for Predicting Performance of Three-Dimensional Pulverized-Fuel Fired Furnaces,'' ASME J. Eng. Gas Turbines Power, **110**, pp. 117–126.

[9] Aoki, H., Tanno, S., Miura, T., and Ohnishi, S., 1992, ''Three-Dimensional Spray Combustion in a Practical Boiler,'' JSME Int. J., Ser. II, **35**, pp. 428–434.

[10] Wiscombe, W. J., 1977, ''The Delta-M Method: Rapid Yet Accurate Radiative Flux Calculations for Strongly Asymmetric Phase Functions,'' J. Atmos. Sci., **34**, pp. 1408–1442.

[11] Lee, H., and Buckius, R. O., 1982, ''Scaling Anisotropic Scattering in Radiation Heat Transfer for a Planar Medium,'' ASME J. Heat Transfer, **104**, pp. 68–75.

[12] Kim, T.-K., and Lee, H. S., 1990, ''Scaled Isotropic Results for Two-Dimensional Anisotropic Scattering Media,'' ASME J. Heat Transfer, **112**, pp. 721–727.

[13] Maruyama, S., 1997, ''Radiative Heat Transfer in a Layer of Anisotropic Scattering Fog Subjected to Collimated Irradiation,'' *Proc., 2nd Int. Symposium on Radiation transfer*, Aug., Kasadasi, Turkey.

[14] Maruyama, S., 1998, ''Radiation Heat Transfer in Anisotropic Scattering Media With Specular Boundary Subjected to Collimated Irradiation,'' Int. J. Heat Mass Transfer, **41**, pp. 2847–2856.

[15] Edwards, D. K., and Balakrishnan, A., 1973, ''Thermal Radiation by Combustion Gases,'' Int. J. Heat Mass Transf., **12**, pp. 25–40.

[16] Hsu, P.-F., Tan, Z., and Howell, J. R., 1992, ''Application of the YIX Method to Radiative Heat Transfer Within a Mixture of Highly Anisotropic Scattering Particles and Non-Gray Gas,'' *Developments in Radiative Heat Transfer*, ASME HTD-Vol. 203, pp. 285–300.

[17] Yuen, W. W., Ma, A. K., and Takara, E. E., 1992, ''Evaluation of Radiative Heat Transfer Using the Generalized Zonal Method and the Absorption Mean Beam Length Concept,'' *Developments in Radiative Heat Transfer*, ASME HTD-Vol. 203, pp. 265–273.

[18] Maruyama, S., Ukaku, M. and Aihara, T., 1995, ''Radiative Heat Transfer of Non-Uniform, Non-Gray, Absorbing, Emitting and Scattering Media Using Band Models,'' *Proc., 32nd National Heat Transfer Symposium of Japan*, Yamaguchi, pp. 591–592.

[19] Siegel, R., and Howell, J. R., 1992, *Thermal Radiation Heat Transfer*, 3rd Edition, Chap. 13, Hemisphere, Washington, DC.

[20] Foster, P. J., and Howarth, C. R., 1968, ''Optical Constants of Carbons and Coals in the Infrared,'' Carbon, **6**, pp. 719–729.

[21] Menguc, M. P., and Viskanta, R., 1985, ''Radiative Transfer in Three-Dimensional Rectangular Enclosures Containing Inhomogeneous, Anisotropically Scattering Media,'' J. Quant. Spectrosc. Radiat. Transf., **33**, pp. 533–549.

[22] Chai, J. C., Lee, H. S., and Patankar, S. V., 1993, ''Ray Effect and False Scattering in the Discrete Ordinates Method,'' Numer. Heat Transfer, Part B, **24**, pp. 373–3899.

[23] Omori, T., Murakami, S., Katoh, S., Choi, C. K., and Kobayashi, H., 1992, ''Coupled Simulation of Convective and Radiative Heat Transfer in Enclosed Space: Accuracy of Shape Factors Obtained by Monte Carlo Method,'' *Proc., Air-Con. Sanit. Eng. Japan*, pp. 653–656.

[24] Smyth, K. C., Miller, J. H., Dorfman, R. C., Mallard, W. G., and Santoro, A. R., 1985, ''Soot Inception in a Methane/Air Diffusion Flame as Characterized by Detailed Species Profiles,'' Combust. Flame, **62**, pp. 157–181.

[25] Maruyama, S., and Wu, H., 2000, ''Comparison of The Absorption Coefficient, Spectral and Total Emissivities of Participating Gases at High Temperature by LBL Analysis and Gas Models,'' *Proc. 4th JSME-KSME Thermal Engineering Conference*, Vol. 1, pp. 223–228.